Research Article

Chun Meng, Yu-Xuan Ren, Fengya Lu, Panpan Yu, Jinhua Zhou and Min-Cheng Zhong*

Constant-force photonic projectile for long-distance targeting delivery

https://doi.org/10.1515/nanoph-2024-0484
Received September 14, 2024; accepted November 11, 2024; published online November 25, 2024

Abstract: Optically controllable delivery of microparticles excites interesting research and applications in various fields because of the noninvasive and noncontact features. However, long-distance delivery with a static low-power light source remains challenging. Here, the constant-force photonic projectile (CFPP) is employed to achieve long-distance delivery of microparticles with a low-power laser beam. The CFPP takes advantage of photon absorption to create a constant optical force within a large range, surpassing traditional tweezers. The concept of CFPP has been experimentally corroborated by remote control over micrometer-sized absorptive particles (APs) using a simple tilted focused beam. At the laser focus, strong photon absorption results in a large constant optical force that ejects the APs along the optical axis. Furthermore, the additional thermal convection field, which attracts particles from a distance into the working range of the CFPP, is utilized to collect the unbound APs for reuse. Finally, we demonstrate the concept of drug delivery by transporting a small microparticle onto a host particle at a remote location. The proposed CFPP provides a new perspective for drug delivery and heat-enhanced photodynamic therapy.

Keywords: optical manipulation; absorbing microparticle; tilted focused beam; optical force; thermal convection; plasmonic gold layer

Chun Meng and Yu-Xuan Ren contributed equally to this work.

***Corresponding author: Min-Cheng Zhong**, Anhui Province Key Laboratory of Measuring Theory and Precision Instrument, School of Instrument Science and Optoelectronics Engineering, Hefei University of Technology, Hefei 230009, Anhui, China, E-mail: zhongmch@hfut.edu.cn. https://orcid.org/0000-0002-9958-192X

Chun Meng and Panpan Yu, Anhui Province Key Laboratory of Measuring Theory and Precision Instrument, School of Instrument Science and Optoelectronics Engineering, Hefei University of Technology, Hefei 230009, Anhui, China, E-mail: mengchun@mail.hfut.edu.cn (C. Meng), yupanpan@hfut.edu.cn (P. Yu).
https://orcid.org/0009-0003-2493-3278 (C. Meng)

Yu-Xuan Ren, Institute for Translational Brain Research, MOE Frontiers Center for Brain Science, Fudan University, Shanghai, 200032, China; and Department of Neurology, Jinshan Hospital, Fudan University, Shanghai, 201508, China, E-mail: yxren@fudan.edu.cn.
https://orcid.org/0000-0002-4641-3148

Fengya Lu and Jinhua Zhou, School of Biomedical Engineering, Anhui Medical University, Hefei 230032, Anhui, China,
E-mail: fylu@ahmu.edu.cn (F. Lu), zhoujinhua@ahmu.edu.cn (J. Zhou)

1 Introduction

The ability to manipulate particles, especially for particle delivery, has fostered researches in materials science, nanotechnology, and biomedical engineering and has also provided the possibility for precise drug delivery and targeted therapy [1], [2]. Diverse approaches using externally controlled stimuli have been proposed for particle delivery, such as dielectrophoresis [3], magnetophoresis [4], acoustic pressure [5], optical force, and hydrodynamic force [6]. Among these approaches, optical methods are particularly popular due to their remote and noncontact feature. Many optical techniques, such as waveguides [7], [8], optical microcavities [9], and plasmons [10], [11], have been developed for the dynamic delivery of particles. However, these technologies rely on prior fabrication of nanostructures, leading to a lack of simplicity, flexibility, and continuity in the control of the delivery distance and direction. Optical trapping is a tool with remote and noncontact operation, and single-particle manipulation precision [12]. The use of piezoelectric devices, such as piezoelectric mirrors [13] and acousto-optic deflectors [14], could help optical tweezers to trap and deliver the particles but require mechanical complexity [13]–[15]. Purely optical methods have been proposed for flexible particle delivery using elliptical beams [16], Bessel-like beams [17], and complex three-dimensional (3D) spatially structured beams [18]. Specifically, the self-accelerating Airy beam can clear the particles in a certain quadrant [19]. However, the particles can only be transported within the limited Rayleigh range of the tightly focused beam because the momentum of particles originates from the transfer of photon momentum. Long-distance transport requires a high-power laser to provide energy, which has low energy efficiency and risk of

photodamage on living organisms. Therefore, it is necessary to investigate a method that achieves long-distance optical delivery of particles at low power.

On the other hand, heat-mediated optical manipulation has widespread application in various fields due to its versatile manipulation capabilities, lower power consumption, and minor photothermal damage [20]. Such techniques for manipulating particles take advantage of the synergistic action of optical forces and various flow field forces, such as Marangoni convection [21], evaporative flow [22], and electro-thermo-plasmonic flow [23]. Among these flow fields, thermal convection has been widely applied for the large-scale assembly of colloidal particles [24]–[26] and the rapid transport of objects toward the plasmonic trapping sites [27]–[29] due to its long working range [30]. Recently, the synergistic effect of thermal convection force and thermophoresis suggests interesting oscillatory motion of microparticles, which may excite advanced biophotonic applications [31]. The thermal convection force originates from the laser heating of a gold film, whose primary function is to pull particles away from the hot spot backward. However, there have been few reports regarding the use of thermal convection for single-particle delivery.

In this paper, we propose a constant-force photonic projectile (CFPP) and have demonstrated its capability for targeting the delivery of microparticles using a tilted focused beam. Near the focus, a constant optical force generated by photon absorption ejects the particle along the beam propagation direction. In addition, the direction and distance of particle delivery can be flexibly controlled by simply adjusting the tilt angle of the optical axis and the laser power. Furthermore, the additional thermal convection force is introduced to collect the particle through a round-trip delivery. This is done by creating a local temperature gradient through resonant plasmonic heating. When the microparticles move out of the range of optical force, thermal convection force will pull the microparticles back into the beam center. Finally, we demonstrate the concept of drug delivery by transporting the microparticles and adhering them to the surface of a larger polystyrene (PS) particle as the target. The proposed CFPP scheme offers the advantages of flexible control, good stability, low power consumption, and long-distance delivery; therefore, it has broad potential in various applications, such as drug delivery or cellular manipulation.

2 Results and discussions

2.1 Principle of constant-force photonic projectile

A tilted beam illuminates the microparticle, whose motion can be classified into four phases under the CFPP (Figure 1(a)). In Phase I, the microparticle is attracted to the beam center due to optical gradient force. In Phase II, the

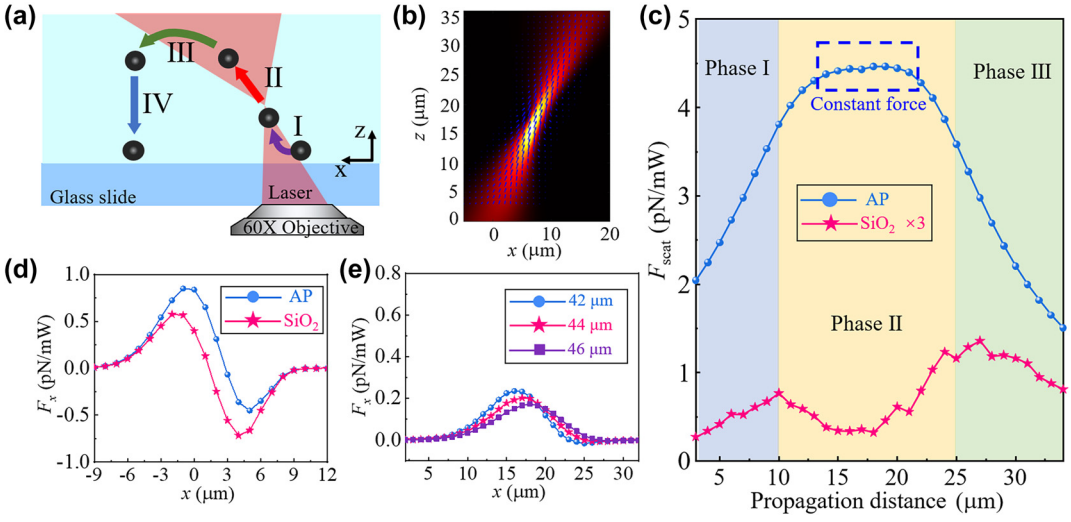

Figure 1: Principle of CFPP. (a) Schematic description of photonic projectile in the x–z plane. The colored arrows indicate the moving trajectory of the microparticle, including attraction (Phase I: purple), ejection (Phase II: red), translation (Phase III: green), and settlement (Phase IV: blue). (b) The optical force field overlaid on the transverse beam profile of the photonic projectile. The color scale represents the relative intensity. The direction and relative length of the arrow represent the direction and relative magnitude of the optical force, respectively. The laser beam is tilted toward the x-axis by an angle of 20°. (c) The axial optical force for the absorbing microparticle and the pure dielectric microparticle. The dashed box represents a large constant force region. The colored shadows correspond to different phases. (d) Transverse force (F_x) on the absorbing microparticle suggests an asymmetric shape on the curve in contrast to the pure dielectric microparticle with the same size at a position ∼8 μm below the focus. (e) Transverse force (F_x) on the absorbing microparticle as a function of the transverse position x at different position z above the focus.

microparticle is accelerated by a constant forward optical force for a long distance along the beam propagation axis and is ejected along the direction of the optical axis. During the ejection process, there is a small thermal gradient force that promotes the ejection of the microparticle. The thermal gradient force originates from the temperature gradient generated on the surface of the microparticle by the laser radiation. In Phase III, the microparticle further moves forward in the transverse plane due to the balance between the upward net force (including the buoyant force, the vertical component of the optical force, and the gravitational force) and the minute transverse optical force. Finally, the microparticle will settle down under the dominant gravitational force in Phase IV.

To better understand how the CFPP works, we performed a finite-difference time-domain (FDTD) simulation to map the transverse beam profile (see Figure 1(b)). In the simulation, a linearly polarized plane wave with $E = \hat{x}E_0 \exp\left(ik_0 z - i\omega t\right)$ tilted with respect to the z axis by an angle of θ illuminates on a microparticle. The optical force ($\boldsymbol{F_O}$) on the particle can be calculated by integrating the Maxwell stress tensor $\boldsymbol{T}$ along a closed boundary ∂S encircling the particle, and the expression is given by [32], [33],

$$\boldsymbol{F_O} = \int_{\partial S} \boldsymbol{T} \cdot \hat{\boldsymbol{n}} \mathrm{d}A, \tag{1}$$

where the Maxwell stress tensor is defined as $T_{ij} = \varepsilon_m\left(E_i E_j - \frac{1}{2}|\boldsymbol{E}|^2\delta_{ij}\right) + \frac{1}{\mu_0}\left(B_i B_j - \frac{1}{2}|\boldsymbol{B}|^2\delta_{ij}\right)$, $\hat{\boldsymbol{n}}$ is the unit vector normal to the enclosing surface, μ_0 is the permeability, and ε_m is the permittivity of the surrounding medium.

To increase the light absorption, we elect to use a hybrid absorbing synthetic particle with magnetite homogenized in the host silica sphere. Different from core–shell APs [34], the Fe_3O_4 nanoparticles are dispersed in a spherical SiO_2 matrix. At a wavelength of 1,064 nm, the refractive indices of SiO_2 and Fe_3O_4 are $n_{SiO2} = 1.45$ and $n_{Fe3O4} = 2.11 + 0.37i$, respectively [35], [36]. The density of absorbing microspheres is approximately 2.6 g/cm^3. The densities of Fe_3O_4 solid crystal and SiO_2 solid crystal are 5.18 g/cm^3 and 2.3 g/cm^3, respectively. The absorbance of the synthetic particle can be controlled by the volume ratio of the silica, specifically, we use APs (Affimag magnetic microspheres, 4.0–5.0 μm in diameter, Base-Line Company, Tianjin) with a volume fraction of $X = 0.9$ for the SiO_2. With $n_{SiO2} = 1.45$ and $n_{Fe3O4} = 2.11 + 0.37i$, the effective refractive index of the microparticle is $n_{eff} = n_{SiO2} \cdot X + (1 - X) \cdot n_{Fe3O4} = 1.516 + 0.037i$ according to the effective medium theory [37].

To understand the force experienced by the AP within the optical field, the optical force field of an AP with a diameter of 4.5 μm is overlaid on the side view profile of the optical field with a tilt angle of $\theta = 20°$ (see Figure 1(b)). The direction and relative length of the arrow represent the direction and relative magnitude of the optical force, respectively. The scattering force, $F_{scatt} = F_y \cos\left(\theta\right) + F_x \sin\left(\theta\right)$ on the AP along the beam axis suggests a large plateau on the top, in contrast, the dielectric silica microparticle experiences a significantly weak scattering force (Figure 1(c)). Since large number of photons are absorbed by the AP, and the energy of the absorbed photons is converted into the kinetic energy of the AP, resulting in a significantly augmented optical scattering force along the direction of light propagation (blue circles in Figure 1(c)). The axial optical force on the AP is increased by a factor of ∼27 as compared with that for the dielectric silica microparticle of the same size. Moreover, the force fluctuation is within 2 % over a distance of ∼10 μm (greater than 3 times the Rayleigh distance) for the synthetic particle. A long-range constant force is conducive to the stable ejection of the microparticle.

For traditional dielectric microparticles, such as silica (refractive index of $n_{SiO2} = 1.45$), the strong optical gradient force at the laser focus dominates, and the scattering force is smaller than the optical gradient force. The transverse optical gradient force may attract both the absorbing and dielectric particles (Figure 1(d)). The horizontal optical force for traditional Gaussian optical tweezers is symmetric at a fixed height since the laser is normally incident. Meanwhile, the particle also experiences forward scattering force (with the same direction as the beam propagation). Once the beam is tilted (as in our CFPP scheme), the scattering force will also contribute to the transverse component, i.e., x-axis. As the particle absorption augments the axial scattering force in the CFPP, the transverse force shifts upward for the APs as compared with the silica particle. As a result, when the normal symmetric curve is shifted upward by a certain amount (determined by the scattering force and the tilt angle), the curve becomes asymmetric. Although the transverse force is asymmetric, it is the major source to collect the surrounding particles to the CFPP as the working particle. The two types of microparticles are both attracted toward the optical axis by the transverse optical force, which corresponds to Phase I.

As the trapping beam diffracts, the transverse force will also decrease. We show that transverse force will still exist for a large transverse range at a longitudinal position over 40 μm, and such minute force will further bring the particles away from the light beam (Phase III). The transverse optical scattering force suggests a weak force along a large area, and such a minute force is sufficient to push the particle forward gently (Figure 1(e)).

2.2 Experimental setup

The photonic projectile was built on an inverted universal infinity-corrected microscope (Figure 2(a)). A 1,064-nm continuous laser (CNI, Changchun, MIL-N-1064, TEM_{00}, CW) with a beam waist diameter of 3 mm is employed for the experiments. The laser beam is apodised to 2 mm with the iris (I) and is focused through a microscope objective (LUMFLN, water immersion, 60×, NA = 1.1, Olympus, Japan) into a diffraction limited spot. The laser beam underfills the pupil of the objective (8 mm); therefore, the numerical aperture (NA) of the objective is not fully utilized. The optical axis of the laser beam can be tilted by the mirrors (Figure 2(a)). The microscopy images are recorded by a CMOS camera (30 frames per second) and saved for offline analysis. The laser power is adjusted by using a power attenuator (PA) and measured at the pupil of the objective using a power meter.

The sample chamber was prepared using a homemade circular trough with an inner diameter of 10 mm and a height of 1 mm between two coverslips (Figure 2(b)). The sample is a diluted suspension of absorbing magnetic microparticles (Part No. 3142, 4.0–5.0 μm diameter magnetic particle, BaseLine, Tianjin), and all the experiments were performed at room temperature.

The tilt angle (θ) refers to the angle of the optical axis relative to the z-axis (Figure 3). We utilize a ZnO nanowire to evaluate the tilt angle of the CFPP. The nanowire can be stably trapped and will align its long axis with the optical axis [38]. The target ZnO nanowire is approximately 15 μm in length (Figure 3(a)). When the optical axis is not tilted (aligned along the z-axis), the trapped ZnO nanowire is observed as a blurry black dot at the center of the observation field (bottom image in Figure 3(b)). Due to the underfilling of the back aperture of the objective, one end of the ZnO nanowire near the laser focus is positioned above the laser focus (top image in Figure 3(b)). In subsequent studies, if not otherwise specified, the projection of the tilted axis onto the x–y plane is set to point toward the positive x-axis.

The tilt angle of the optical axis depends on the position of laser incidence into the objective lens, which can be adjusted by changing the angle of the mirrors. The further the laser incidence position deviates from the center of the objective lens, the larger the magnitude of θ. When the optical axis is tilted, the trapped ZnO nanowire aligns itself with the optical axis (see Figure 3(c)). As the length of the nanowire is larger than the axial field of view of the microscopy, only one end of the nanowire can be clearly visualized. Although the other end of the nanowire is blurred, we can estimate the centroid of the other end with considerably good resolution. The length can be measured when the nanowire aligns itself within the transverse plane; therefore, we can estimate the tilt angle through the nanowire orientation. When the edge of the incident light reaches the edge of the objective lens, the projected length of the trapped ZnO nanowires in the x–y plane is approximately 5.4 μm. The maximum tilt angle is estimated to be $\theta \approx 20°$. Although the tilt angle is not of high resolution, it offers a good estimate to configure the setup.

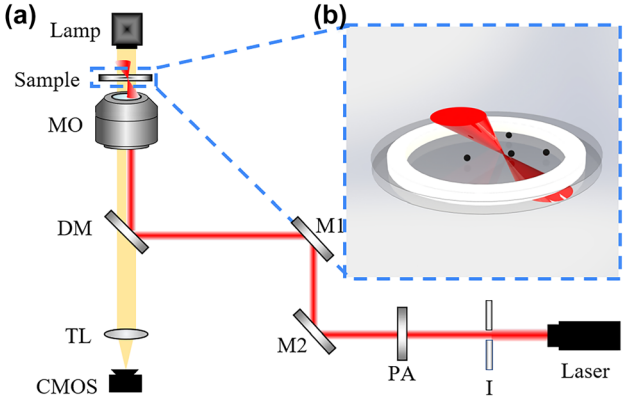

Figure 2: Experimental setup. (a) A 1,064 nm laser is utilized as the trapping beam. The iris (I) eliminates the high-order parasitic mode, while the power is adjusted by a variable power attenuator (PA). The tilt angle of the photonic projectile is fine-tuned by the mirror pair M1 and M2. The LED illuminates the sample, and the image is collected by a CMOS camera through an objective (MO) and tube lens (TL). The dichroic mirror (DM) reflects the trapping beam and coaligns with the illumination beam. (b) The diluted suspension of the microparticle inside the chamber.

2.3 CFPP for delivery of micrometer-sized APs

We report the CFPP for delivery of an AP under the radiation of a tilted laser beam (Figure 4(a) and Supplementary Movie S1). The positions of the microparticle as a function of time in the x-direction and y-direction are depicted in Figure 4(b) and (c), respectively. The coordinate origin ($x = 0$, $y = 0$) is set at the beam focus projected onto the x–y plane. The tilt angle of the optical axis is 20°. The laser focus is at a height of 8 μm above the bottom surface of the sample chamber. The laser power is 60 mW. In Phase I, the microparticle moves toward the focus under the optical force (Snapshots 1–3). Microparticle image blurring indicates that the particle is above the imaging plane. In Phase II, near the focus, the microparticle is subjected to a large long-range constant optical force. The direction of the optical force is consistent with the optical axis, causing the microparticle to be ejected and leaving the focus along the direction relative to the optical axis (Snapshots 3–4).

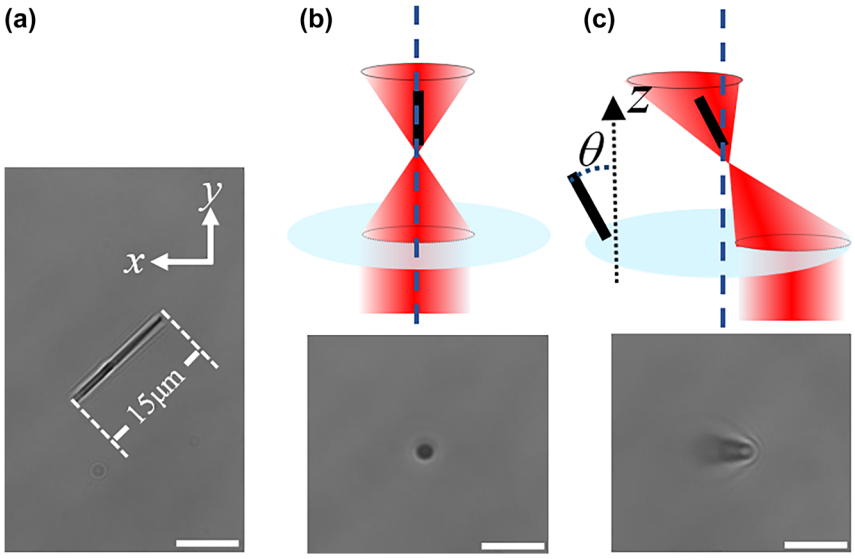

Figure 3: Directional control of a ZnO nanowire. The observation plane of the experimental phenomenon is the x–y plane. Scale bar, 8 μm. (a) The target ZnO nanowire laid on the coverslip suggests a length of 15 μm. (b) The long axis of the ZnO nanowire is aligned with the trapping beam propagation axis. (c) The ZnO nanowire tilts its long axis inside the photonic projectile. The tilt angle of the ZnO nanowire with respect to the z-axis direction is θ. The blue dashed line represents the symmetry axis of the objective.

Meanwhile, due to the laser focusing on the surface of the microparticle, the microparticle is subjected to the action of a thermal force induced by the temperature gradient. The direction of the temperature gradient force is consistent with the optical axis; therefore, it has a positive effect on the ejection of the microparticle. The maximum velocity of the microparticle in the x-direction reached 198 μm/s. In Phase III, when the microparticle moves away from the focus, the optical force on the microparticle surface rapidly decreases. The optical force cannot overcome the viscous resistance, leading to a rapid decrease in the microparticle velocity (Snapshots 4–5). Subsequently, the microparticle is further pushed away from the focus by the optical force along the optical axis (Snapshots 5–6). During this process, because the microparticle is far from the laser focus, the optical force exerted on the microparticle along the x-direction is small. The magnitude of the microparticle's velocity in the x-direction is on the order of 1 μm/s. In Phase IV, when the

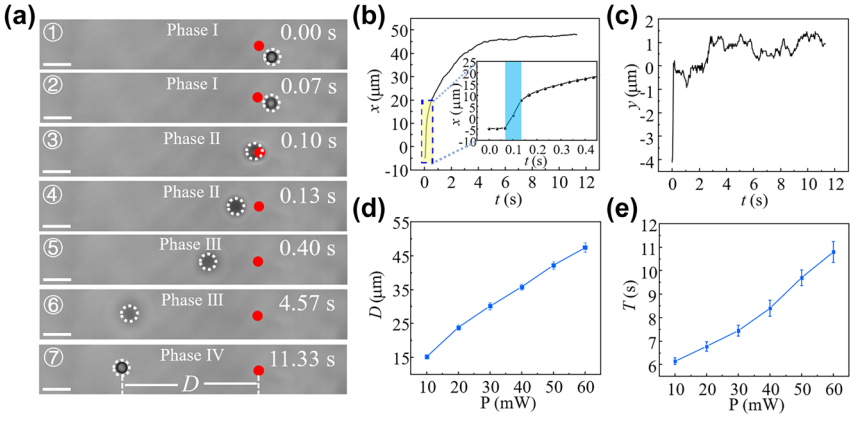

Figure 4: Delivery of the micrometer-sized APs. (a) Image snapshots from the video (see Movie S1). The focus is 8 μm above the bottom surface. The tilt angle of the optical axis is ∼20°. The red dots indicate the projection of the focal spot onto the x–y plane. Scale bar, 10 μm. (b) The position of the AP as a function of time in the x-direction. The inset indicates a zoom-in view of the yellow region. The blue-shaded area represents the region where a constant optical force is applied during the ejection process. (c) The position of the AP as a function of time in the y-direction. The laser power is 60 mW. The position $(x, y) = (0, 0)$ represents the projection of the focal spot onto the x–y plane. (d) The value of D as a function of laser power. D is the distance along the x-direction from the position where the AP falls to the bottom to the projected position of the focal spot on the bottom surface (see Figure 4(a)). (e) The delivery period T as a function of laser power. Each power has at least 6 delivery events involving the same particle.

particle moves out of the range of optical force, there is almost no displacement in the x-direction on the particle (see Figure 4(b)). Finally, the microparticle settles down to the bottom substrate due to gravity (Snapshots 6–7). The direction of microparticle transport projected onto the horizontal plane is basically consistent with the direction of the optical axis projected onto the horizontal plane (see Figure 4(c)). Therefore, the direction of microparticle transport can be controlled by the direction of the beam axis.

We evaluate the transport ability by separation of the farthest location of the particle to the laser focus along the x-direction, i.e., D. The delivery of the AP depends on the laser power. In the experiments, the values of D and the delivery period T were measured at different laser powers (Figure 4(d) and (e)). As the laser power increases, both of the distance D and period T increase. Larger power leads to an increase in the optical force. At the same time, the higher laser power creates a larger local temperature gradient in the AP surface, resulting in an increased thermal gradient force. The larger optical and thermal gradient forces in the x-direction propel the particle even farther from the focus spot. Similarly, the larger optical and thermal gradient forces in the z-direction result in particle transport in the higher horizontal plane. When the particle is attracted close to the optical axis, the side closer to the optical axis is heated, resulting in a thermal gradient force, with its component in the x-direction opposing the optical force in the x-direction.

When the laser power exceeds 65 mW, the particles are attracted near the optical axis and then rapidly pushed out of the range of optical force, rather than being attracted to the focus (see Movie S2). The motion of the particle is two-dimensional. The forces acting on the particle in the horizontal direction include the optical force pointing toward the optical axis and the thermal gradient force in the opposite direction. This phenomenon can be reasonably explained as the thermal gradient force exceeding the horizontal component of the optical force at the position where the motion direction changes, and the net external force acting on the particle in the vertical direction is insufficient to overcome gravity. When the laser power is reduced to 4 mW, the particle is trapped at the mechanical equilibrium above and to the left of the focus (see Movie S3). In the x-direction, the optical force balances with the thermal gradient force. In the z-direction, the optical and thermal gradient forces can balance gravity. However, the trapping forces are very tiny due to low laser power, so such trapping is easily disrupted by Brownian motion and convection disturbances. When the laser power decreases to 1 mW, the external forces on the microparticle are not sufficient to overcome gravity, so the microparticle is trapped at the bottom surface of the sample chamber, where the optical and thermal gradient forces are balanced. Similar phenomenon has been found in the previous studies [34], [39].

Combining experiments with simulations, we discuss the forces acting on the microparticles during the CFPP process. In the x–y plane, due to the target position of the delivery being in the x-direction of the focus, we mainly study the force situation of the particles in the x-direction. Here, we choose the example with an incident power of 60 mW. The experimentally measured transmittance coefficient of the microscope objective is 0.4, so the effective optical power acting on the microparticle is only 24 mW. In previous studies [40], when the laser power is 20 mW, the thermal gradient force experienced by the microparticle was estimated to be 0.2 pN, which is much smaller than the optical force (Figure 1(e)). When the microparticle moves away from the focus, the temperature gradient on the surface of the microparticle is negligible. Therefore, during the delivery process, the microparticle is primarily influenced by the optical force. Due to the small mass of the microparticle (124 pg), even if the magnitude of the acceleration of the microparticle reaches 1 mm/s^2, the magnitude of the net external force acting on the microparticle is only on the order of 0.1 fN. Therefore, the values of thrust (including F_o and F_t) and viscous drag force ($F_d = 6\pi\eta r v$, where η is the viscosity coefficient, r is the radius of the particle, and v is the relative velocity between the particle and the flow field) experienced by the particle during its movement are approximately balanced by each other. During the ejection process (Snapshots 3–4 in Figure 4(a)), the maximum velocity of the microparticle in the x-direction is 198 μm/s. The maximum optical force experienced by the microparticle is approximately 7.6 pN. The maximum optical force experienced by the microparticle has a constant force region near 0.1 s, with an interval length of approximately 6 μm (see Figure 4(b)), which is on the same order of magnitude as the constant force interval length obtained in the simulation (see Figure 1(e)). When $t = 0.5$ s, the microparticle moves to the position $(x, z) = (19, 38)$ μm. Based on the experimentally measured velocity of $v = 15$ μm/s at this position, the optical force experienced by the microparticle is 0.57 pN, well consistent with the simulation in terms of the order of magnitude (the optical force at this position is 1.44 pN in simulation).

Particle acceleration techniques, as tools for precise manipulation and analysis of microscopic matter, are widely applied in materials science, medical treatment, and fundamental physics. In recent years, with the advancement of nanotechnology and photonics, particle acceleration using low-power lasers has become a hot topic. For

instance, by utilizing optical gradient forces in metallic V-grooves, nanoparticles in air can be accelerated to speed of several centimeters per second [41]. Recently, research by Kislov et al. further demonstrated that using picosecond-scale thermal expansion effects, particles in air can be accelerated to speed of 15 m/s under the action of low-power lasers [42]. This discovery brings new possibilities to the research field of particle acceleration, especially in applications requiring noninvasiveness and precise control. With our proposed CFPP, under the action of a low-power laser, APs in water are accelerated to 198 um/s by optical forces. If our scheme is applied in air, where there is no resistance from the water viscosity, the speed of particles could be further increased. The large constant force working area induced by light absorption, which far exceeds that of traditional optical tweezers, has not been mentioned in these studies on particle acceleration. Compared to these researches, the fully optically controllable scheme is more flexible, and particles show no significant deformation or damage.

One promising example is the particle delivery, which plays a crucial role in drug delivery, as they can transport drug precisely to target cells or tissues, thereby improving therapeutic efficacy. Furthermore, due to the requirement that the particle at the bottom must be within the range of optical force for delivery, the limited range of optical force restricts its application. On the other hand, after transport, the particle will move out of the range of optical force. For a fixed light source, this is unfavorable for the reuse of the particle. In the following, an additional thermal convection force is applied to collect the micrometer-sized AP at a much broader range.

2.4 Circulating micrometer-sized APs with thermal convection

Since the optical gradient force acts in a limited range around the trapping beam. To collect microparticles in a larger range for the CFPP, an additional thermal convection force is employed to drag the particles back into the range of the optical gradient force. The local thermal convection can be induced by creating localized temperature gradients [28], [29], [31]. In particular, a gold film with a thickness of about 10 nm was deposited on the bottom surface of the chamber (Figure 5(a)). The laser beam irradiates the gold film, converting some of the light energy into thermal energy, thereby creating a local temperature gradient and inducing thermal convection. Near the bottom surface of the chamber, the direction of thermal convection points toward the heating point, and the range of thermal convection force is much greater than the maximum distance of particle delivery. The observed flow pattern of the thermal convection is well consistent with the previous reports [28], [29], [31].

Combined with the plasmonics-mediated thermal convention force, the CFPP can circulate the APs over a larger area. The round-trip delivery of micrometer APs can be schematically illustrated in the x–z plane (Figure 5(a)). Figure 5(b) shows representative snapshots of the motion

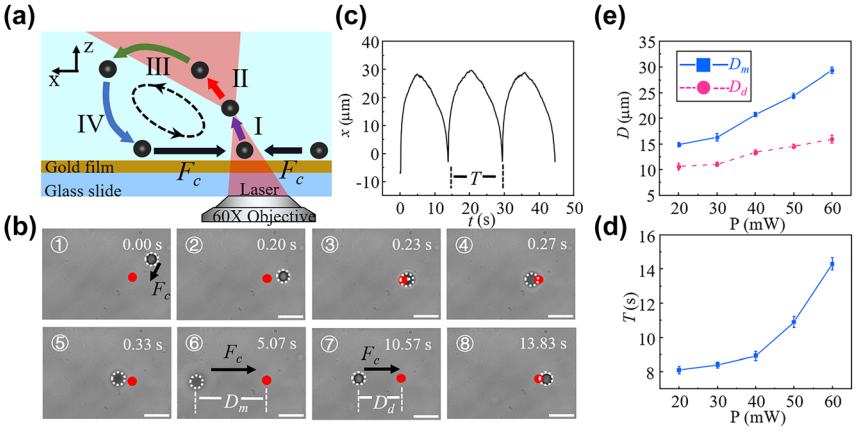

Figure 5: Plasmonics mediated delivery of micrometer-sized APs. (a) Schematic description of round-trip delivery. The particle in the chamber moves along the arrows. The bottom of the sample cell is coated with a 10 nm thick gold film. The microparticle out of range of optical force is attracted to the hotspot under the thermal convective force (Fc) (black arrows). The correspondence between the other colored arrows and phases is consistent with Figure 4(a). (b) (See Movie S4) Images of the microparticle at different time points (Snapshots 1—8). The red point indicates the projection of the focal spot onto the x–y plane. Scale bar, 10 μm. The tilt angle of the optical axis is 20 deg. (c) The position of the microparticle as a function of time in the x-direction. The position $(x, y) = (0, 0)$ represents the coordinates of the projected focus onto the x–y plane. The laser power is 60 mW. (d) The values of D_m and D_d as a function of laser power. D_d is the distance in the x-direction from the position where the AP falls to the bottom surface to the projected position of the focal spot on the surface. D_m is the farthest distance in the x-direction between the microparticle and the focal spot during particle motion. (e) The round-trip delivery period T as a function of laser power. Each power has at least 6 delivery events involving the same particle.

of the microparticle (Snapshots 1–8) (see Movie S4). The laser power was 60 mW. Correspondingly, the positions of the microparticle as a function of time in the x-direction are depicted in Figure 5(c). At the beginning, the thermal convection force (F_c) induced by the laser heating of the gold film attracts the microparticle beyond the range of optical forces to the hot spot (Snapshots 1–2), which is within the scope of the optical force. Under the action of a tilted-focused laser beam, the microparticle is subjected to attraction (Phase I, Snapshots 2–4), ejection (Phase II, Snapshots 4–5), and repulsion (Phase III, Snapshots 5–6), which is similar to the microparticle motion described in Section 2.3. When the microparticle moves to the farthest position D_m from the focal point (position 6), it will be out of the range of optical force. Then, the microparticle settles to the lower substrate of the sample cell under the action of gravity (Phase IV, Snapshots 6–7). Different from the microparticle motion described in Section 2.3, during the settlement, the microparticle is dragged by the thermal convection toward the heating point, leading to a displacement difference between the farthest position D_m and the position D_d of the microparticle reaching the bottom surface. In practical operation, the displacement difference ($D_m - D_d$) can be reduced by properly switching the laser. Subsequently, the microparticle returns to the heating point under the action of the thermal convection force (position 8). When the laser operates continuously, the microparticle will continue to move back and forth along the trajectory from position 2 to 8 (see Movie S2). In the process of moving away from the focus (Snapshots 4–6), the component of the thermal convective force in the x-direction is positive, promoting the further transport of the microparticle. In the experiment, the transmission coefficient of the gold film is measured to be approximately 0.4. Therefore, when the laser power is 60 mW, the actual laser power acting on the particles is 9.6 mW. Compared to the case without thermal convective force (maximum transport distance of 26.4 μm obtained from Figure 4(d)), the farthest transport distance of the microparticle in the x-direction is greater (maximum transport distance of 29.6 μm obtained from Figure 5(c)).

The delivery of the microparticle depends on the laser power. As the laser power increases, the value of D_m and D_d increases (see Figure 5(d)). Under the influence of the thermal convective force, the microparticle moves closer to the heating point during the settlement process, leading to D_d being smaller than D_m. With the laser power increasing, the microparticles are pushed to a larger height, while the increased temperature gradient induces a stronger thermal convection force, resulting in a larger displacement difference ($D_m - D_d$). When the laser is in continuous operation, the microparticle moves back and forth with a period T. The greater the laser power acting on the microparticles, the further they are pushed, and the longer the period of back-and-forth motion. Therefore, when the laser power is in the range of 20–60 mW, the value of T increases with the increase of laser power (Figure 5(e)). When the laser power exceeds 64 mW, localized overheating of the water generates microbubbles. The maximum temperature on the surface of the gold film is estimated to be 373.15 K at a laser power of 64 mW, which is close to the maximum temperature (371.2 K) we measured using 5CB [28], [29]. This indicates the reliability of the experimental data. When the laser power is reduced to 14 mW, the farthest position of the transmission ($D_m = 5.5$ μm) is close to the laser focus, the microparticle passes through a position where the upward net force and gravity are equal during the falling process, causing the particle to briefly pause during the descending. Due to thermal convection disturbance, the particle cannot be stably trapped and eventually falls to the bottom surface. When the laser power is below 11 mW, the upward net force on the microparticle is smaller than the gravity, so the microparticle is trapped at the bottom of the sample cell near the hot spot. The trapping forces are the horizontal thermal convection force and the optical gradient force.

Compared to particle delivery driven by pure optical force [17], [43], [44], the combination of CFPP technology with a thermal convection field has shown some advantages. Firstly, transport by pure optical force requires particles to be captured in an optical trap, and the particle suffers from a strong irradiation of light exposure and photodamage. However, tilted focused beam can be used to transport AP along long distance with constant force and significantly reduced power density. Secondly, the performance of traditional optical tweezers varies with particles of different size. The Brownian motion of smaller particles is more intense, leading them to escape from traps, which is not conducive to particle delivery. In our scheme, there is no need to capture the particles, thus relatively reducing the requirements for the laser. Thirdly, transport by pure optical force requires particles to be within the range of the optical force, which limits its application. However, in our scheme, the addition of thermal convection greatly expands the area of transportable particles. Our scheme also has some limitations. The higher local temperature restricts the types of particles that can be transported. Moreover, as compared to the transport of particles along adjustable 3D paths using structured light beams [44], in our scheme, the particles' movement is along a fixed direction. Therefore, the proposed scheme would be preferentially easier to control the probe particle to the target with better resolution.

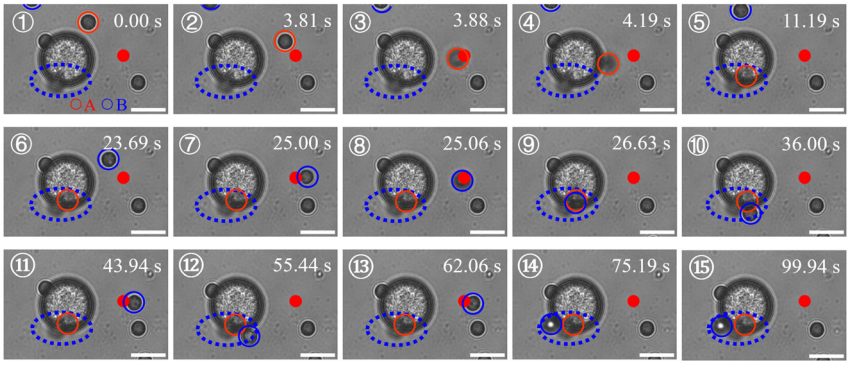

Figure 6: Delivery of micrometer-sized APs to a targeting object region (see Movie S5). The bottom surface of the chamber is coated with a 10 nm-thick gold film. The area marked with blue dashed lines is the target location of delivery. The red point indicates the projection of the focal spot onto the x–y plane. The red and blue circles represent microparticles A and B, respectively. Scale bar, 10 μm.

The combination of CFPP technology and thermal convective force allows for the reproducible manipulation of the same microparticle. In principle, we want the drug-carrying particle to be delivered to the target region, and bound on the target to release drug. There are chances that the particle cannot be effectively bound on the target (off-target) and will be wandering around the normal tissue/cells to infect on the normal tissue. With the circular manipulation, we are able to collect all those off-targeted particles. These capabilities suggest potential applications in efficient drug delivery while avoiding photothermal damage to surrounding healthy tissues. Periodic back-and-forth transportation can be used for intermittent drug delivery and ensuring the high efficacy of the targeted delivery. Conceptual experiments are provided in Section 2.5. Future research can focus on optimizing the parameters of CFPP and thermophoretic forces for specific drug delivery tasks, as well as exploring the compatibility of this approach with various drug formulations and biological systems.

2.5 Delivery of the micrometer-sized APs to a targeting object

The CFPP can be utilized for targeted delivery. To this end, we use a large PS microparticle with a diameter of 15 μm (Figure 6 and Movie S5) as the target. Two micrometer-sized APs (marked by blue and red circles) at different initial positions can be delivered to the bottom of the target particle (labeled by the blue dashed ellipse). The bottom surface of the chamber is coated with a 10 nm-thick gold film. Initially, the microparticles A (red circle) is attracted to the heating point by the thermal convection force (Snapshots 1–2). Once the microparticle enters the range of the CFPP, it will be delivered to the targeting PS microparticle and adheres on the surface of the PS microparticle (Snapshots 4–15). However, the spontaneous adsorption of particles onto the PS microparticle surface is not guaranteed especially when the AP is not chemically treated on the surface. This necessitates the recovery of nonadsorbed particles and the reuse until they adhere to the PS microparticle surface. This is experimentally corroborated by the delivery of microparticle B, which is attracted to the center of the CFPP by the thermal convection force (Snapshots 1–7). Afterward, microparticle B is delivered to the targeting area on the PS microparticle (Snapshots 8–9). However, unlike microparticle A, microparticle B does not adhere to the PS microparticle surface but is instead attracted back to the heating source by the thermal convection forces (Snapshots 10–11). The microparticle B is delivered repeatedly for two more times (Snapshots 11–14). Ultimately, microparticle B adheres to the PS microparticle surface (Snapshots 14–15). Therefore, the proposed delivery scheme may be helpful to deliver drug particles accurately and flexibly and can additionally enhance the probability of their adhesion to target objects to diseased tissues effectively.

In practice, the probe for the targeting delivery may be coated with chemicals that bind with the target region easily. Therefore, the developed CFPP may potentially be used to deliver drug for precision medicine. The addition of the thermal convection force, however, can collect those off-targeting particles back to the range of CFPP, ensuring the high efficacy of the targeted delivery.

3 Conclusions

In conclusion, we propose the CFPP to deliver the microparticle with a tilted-focused laser beam and achieve long-distance controllable delivery of the AP using the CFPP technology. In theory, the directional delivery of the AP along a direction relative to the optical axis can be achieved under the action of optical forces. The AP experiences a large constant optical force along the optical axis across the focus, and the width of the constant force along the direction of light propagation extends up to 10 μm. By comparing the optical force experienced by pure dielectric microparticles,

we point out that such a constant optical force originates from the absorption of photons. The long-distance delivery of the AP is experimentally corroborated with AP with a diameter of 4.5 μm using a low-power focused laser beam tilted by an angle of 20°. Consistent with the FDTD simulation, the microparticle is ejected by a large constant optical force near the focus, reaching a maximum ejection velocity of 198 μm/s, and the range of the constant force in the *x*-direction is ∼6 μm, which makes the delivery of microparticles more stable. The range of the CFPP can be further increased by light-controlled thermal convection mediated by a thin layer of gold film using laser irradiation. The thermal convection force attracts the particles near the bottom of the chamber to the heating source, even if the particles are beyond the range of the optical force. Finally, the APs are delivered and adhered to the surface of a large-sized PS particle. The heat-mediated CFPP approach enables repeated delivery of unbound APs as long as the binding strength between the AP and the target particle is insufficient. The collection of the unbound AP to the CFPP range enhances the efficacy of particle delivery.

Moreover, the delivery distance and direction can be adjusted by the laser power and the tilt angle of trapping beam, respectively. This approach has the advantages of easy operation, high-efficiency, and low cost compared to the techniques using spatial light manipulation [44] and using nanostructure [45]. It is worth mentioning that light absorption generates a large constant optical force area, enabling efficient acceleration and precise control of particles, which may have potential applications in particle manipulation and measurement fields. In addition, the CFPP allows for the delivery of the APs to positions beyond the normal laser diffraction range, effectively avoiding photon damage at the target location. The advantage of CFPP for delivery is simplicity, flexibility, and controllability, and minimum photon damage at the target location, offering potential applications in the fields of drug delivery, photothermal therapy, and bioassays. With its noninvasive nature, fully optical control, and low laser power driving features, CFPP technology has the potential applications in the field of biomedicine. Although the currently proposed the CFPP technology is mainly applicable to absorptive particles, we are working on to expand the broadband applicability for transparent and biological samples. Some schemes are provided to expand the scope of CFPP technology, such as surface modification or doping to enhance the particle's light absorption capability, or the use of a different light wavelength in the infrared region.

Research funding: This work was supported by National Natural Science Foundation of China (Grant Nos. 11874138, 12204456, 62475047), Fundamental Research Funds for the Central Universities (JZ2024HGTB0260), Open Project of Advanced Laser Technology Laboratory of Anhui Province (AHL2022KF02).

Author contribution: Chun Meng and Yu-Xuan Ren contributed equally to this work. All authors have accepted responsibility for the entire content of this manuscript and approved its submission.

Conflict of interest: Authors state no conflicts of interest.

Data availability: All data that support the findings of this study are included in the paper.

References

[1] S. Das, *et al*., "Harnessing catalytic pumps for directional delivery of microparticles in microchambers," *Nat. Commun.*, vol. 8, no. 1, p. 14384, 2017.

[2] S. Wilhelm, *et al*., "Analysis of nanoparticle delivery to tumours," *Nat. Rev. Mater.*, vol. 1, no. 5, p. 16014, 2016.

[3] M. D. Pysher and M. A. Hayes, "Electrophoretic and dielectrophoretic field gradient technique for separating bioparticles," *Anal. Chem.*, vol. 79, no. 12, pp. 4552—4557, 2007.

[4] J. Nguyen, D. V. Conca, J. Stein, L. Bovo, C. A. Howard, and I. Llorente Garcia, "Magnetic control of graphitic microparticles in aqueous solutions," (in eng), *Proc. Natl. Acad. Sci. U. S. A.*, vol. 116, no. 7, pp. 2425—2434, 2019.

[5] K. J. Rao, F. Li, L. Meng, H. Zheng, F. Cai, and W. Wang, "A force to be reckoned with: a review of synthetic microswimmers powered by ultrasound," *J. Opt. Soc. Am.*, vol. 11, no. 24, pp. 2836—2846, 2015.

[6] M. Solsona, E. Y. Westerbeek, J. G. Bomer, W. Olthuis, and A. van den Berg, "Gradient in the electric field for particle position detection in microfluidic channels," *Lab Chip*, vol. 19, no. 6, pp. 1054—1059, 2019.

[7] A. H. J. Yang, S. D. Moore, B. S. Schmidt, M. Klug, M. Lipson, and D. Erickson, "Optical manipulation of nanoparticles and biomolecules in sub-wavelength slot waveguides," *Nature*, vol. 457, no. 7225, pp. 71—75, 2009.

[8] G. Wang, Z. Ying, H.-P. Ho, Y. Huang, N. Zou, and X. Zhang, "Nano-optical conveyor belt with waveguide-coupled excitation," *Opt. Lett.*, vol. 41, no. 3, pp. 528—531, 2016.

[9] M. D. Baaske, M. R. Foreman, and F. Vollmer, "Single-molecule nucleic acid interactions monitored on a label-free microcavity biosensor platform," *Nat. Nanotechnol.*, vol. 9, no. 11, pp. 933—939, 2014.

[10] P. Hansen, Y. Zheng, J. Ryan, and L. Hesselink, "Nano-optical conveyor belt, part I: theory," *Nano Lett.*, vol. 14, no. 6, pp. 2965—2970, 2014.

[11] Y. Zheng, J. Ryan, P. Hansen, Y.-T. Cheng, T.-J. Lu, and L. Hesselink, "Nano-optical conveyor belt, part II: demonstration of handoff between near-field optical traps," *Nano Lett.*, vol. 14, no. 6, pp. 2971—2976, 2014.

[12] A. Ashkin, "Acceleration and trapping of particles by radiation pressure," *Phys. Rev. Lett.*, vol. 24, no. 4, pp. 156—159, 1970.

[13] C. Mio, T. Gong, A. Terray, and D. W. M. Marr, "Design of a scanning laser optical trap for multiparticle manipulation," *Rev. Sci. Instrum.*, vol. 71, no. 5, pp. 2196—2200, 2000.

[14] S. F. Tolić-Nørrelykke, E. Schäffer, J. Howard, F. S. Pavone, F. Jülicher, and H. Flyvbjerg, "Calibration of optical tweezers with positional detection in the back focal plane," *Rev. Sci. Instrum.*, vol. 77, no. 10, p. 103101, 2006.
[15] K. Sasaki, M. Koshioka, H. Misawa, N. Kitamura, and H. Masuhara, "Pattern formation and flow control of fine particles by laser-scanning micromanipulation," *Opt. Lett.*, vol. 16, no. 19, pp. 1463—1465, 1991.
[16] Z. Che, *et al*., "Distance-controllable and direction-steerable opto-conveyor for targeting delivery," *Photonics Res.*, vol. 8, no. 7, pp. 1124—1133, 2020.
[17] H. Lee, M. Lee, H. J. Lee, J. Yoon, K. Dholakia, and K. Oh, "Optical transport over millimeter distances of a microscopic particle using a novel all-fiber Bessel-like beam generator," *Opt. Lasers Eng.*, vol. 165, no. 1, p. 107549, 2023.
[18] J. A. Rodrigo and T. Alieva, "Freestyle 3D laser traps: tools for studying light-driven particle dynamics and beyond," *Optica*, vol. 2, no. 9, pp. 812—815, 2015.
[19] J. Baumgartl, M. Mazilu, and K. Dholakia, "Optically mediated particle clearing using airy wavepackets," *Nat. Photonics*, vol. 2, no. 11, pp. 675—678, 2008.
[20] Z. Chen, J. Li, and Y. Zheng, "Heat-mediated optical manipulation," *Chem. Rev.*, vol. 122, no. 3, pp. 3122—3179, 2022.
[21] A. W. Hauser, S. Sundaram, and R. C. Hayward, "Photothermocapillary oscillators," *Phys. Rev. Lett.*, vol. 121, no. 15, p. 158001, 2018.
[22] N.-A. Goy, N. Bruni, A. Girot, J.-P. Delville, and U. Delabre, "Thermal Marangoni trapping driven by laser absorption in evaporating droplets for particle deposition," *Soft Matter*, vol. 18, no. 41, pp. 7949—7958, 2022.
[23] Y. Liu, *et al*., "Nanoradiator-mediated deterministic opto-thermoelectric manipulation," *ACS Nano*, vol. 12, no. 10, pp. 10383—10392, 2018.
[24] B. Zhang, X.-F. Zhang, M. Shao, C. Meng, F. Ji, and M.-C. Zhong, "An opto-thermal approach for assembling yeast cells by laser heating of a trapped light absorbing particle," *Rev. Sci. Instrum.*, vol. 94, no. 3, p. 034105, 2023.
[25] V. Muraveva, M. Bekir, N. Lomadze, R. Großmann, C. Beta, and S. Santer, "Interplay of diffusio- and thermo-osmotic flows generated by single light stimulus," *Appl. Phys. Lett.*, vol. 120, no. 23, p. 231905, 2022.
[26] F. Lu, *et al*., "Controllable optofluidic assembly of biological cells using an all-dielectric one-dimensional photonic crystal," *Photonics Res.*, vol. 10, no. 1, pp. 14—20, 2021.
[27] J. Chen, *et al*., "Highly-adaptable optothermal nanotweezers for trapping, sorting, and assembling across diverse nanoparticles," *Adv. Mater.*, vol. 36, no. 9, p. 2309143, 2023.
[28] J. Chen, *et al*., "CRISPR-powered optothermal nanotweezers: diverse bio-nanoparticle manipulation and single nucleotide identification," *Light Sci. Appl.*, vol. 12, no. 1, p. 273, 2023.
[29] M. Franzl and F. Cichos, "Hydrodynamic manipulation of nano-objects by optically induced thermo-osmotic flows," *Nat. Commun.*, vol. 13, no. 1, p. 656, 2022.
[30] J. S. Donner, G. Baffou, D. McCloskey, and R. Quidant, "Plasmon-assisted optofluidics," *ACS Nano*, vol. 5, no. 7, pp. 5457—5462, 2011.
[31] C. Meng, F. Lu, N.-Q. Zhang, J. Zhou, P. Yu, and M.-C. Zhong, "Optothermal microparticle oscillator induced by Marangoni and thermal convection," *Langmuir*, vol. 40, no. 14, pp. 7463—7470, 2024.
[32] J. D. Jackson, *Classical Electrodynamics*, 3rd ed. New York, John Wiley & Sons, 1999.
[33] Y.-X. Ren, *et al*., "Topologically protected optical pulling force on synthetic particles through photonic nanojet," *Nanophotonics*, vol. 13, no. 2, pp. 239—249, 2024.
[34] M. C. Zhong, A. Y. Liu, and F. Ji, "Opto-thermal oscillation and trapping of light absorbing particles," *Opt. Express*, vol. 27, no. 21, pp. 29730—29737, 2019.
[35] M. A. Ordal, R. J. Bell, R. W. Alexander, Jr., L. L. Long, and M. R. Querry, "Optical properties of fourteen metals in the infrared and far infrared : Al, Co, Cu, Au, Fe, Pb, Mo, Ni, Pd, Pt, Ag, Ti, V, and W," *Appl. Opt.*, vol. 24, no. 24, p. 4493, 1985.
[36] I. H. Malitson, "Interspecimen comparison of the refractive index of fused silica," *J. Opt. Soc. Am.*, vol. 55, no. 10, pp. 1205—1209, 1965.
[37] A. Girot, *et al*., "Motion of optically heated spheres at the water-air interface," *Langmuir*, vol. 32, no. 11, pp. 2687—2697, 2016.
[38] P. J. Pauzauskie, A. Radenovic, E. Trepagnier, H. Shroff, P. Yang, and J. Liphardt, "Optical trapping and integration of semiconductor nanowire assemblies in water," *Nat. Mater.*, vol. 5, no. 2, pp. 97—101, 2006.
[39] F. Li, *et al*., "Thermo-optical tweezers based on photothermal waveguides," *Microsyst. Nanoeng.*, vol. 10, no. 1, p. 123, 2024.
[40] W. Bai, M. Shao, J. Zhou, Q. Zhao, F. Ji, and M.-C. Zhong, "An approach of bubble generation and manipulation by using the photothermal effects of laser irradiation on light absorbing particles," *Rev. Sci. Instrum.*, vol. 92, no. 11, p. 114902, 2021.
[41] A. S. Shalin and S. V. Sukhov, "Plasmonic nanostructures as accelerators for nanoparticles: optical nanocannon," *Plasmonics*, vol. 8, no. 2, pp. 625—629, 2013.
[42] D. Kislov, *et al*., "Optothermal needle-free injection of vaterite nanocapsules," *Adv. Sci.*, vol. 11, no. 5, p. 2305202, 2024.
[43] M. M. Shanei, E. Engay, and M. Käll, "Light-driven transport of microparticles with phase-gradient metasurfaces," *Opt. Lett.*, vol. 47, no. 24, pp. 6428—6431, 2022.
[44] J. A. Rodrigo, M. Angulo, and T. Alieva, "All-optical motion control of metal nanoparticles powered by propulsion forces tailored in 3D trajectories," *Photonics Res.*, vol. 9, no. 1, pp. 1—12, 2021.
[45] J. C. Ndukaife, A. V. Kildishev, A. G. Nnanna, V. M. Shalaev, S. T. Wereley, and A. Boltasseva, "Long-range and rapid transport of individual nano-objects by a hybrid electrothermoplasmonic nanotweezer," *Nat. Nanotechnol.*, vol. 11, no. 1, pp. 53—59, 2016.

Supplementary Material: This article contains supplementary material (https://doi.org/10.1515/nanoph-2024-0484).